# Lyotropic Phase Behavior of Poly(ethylene oxide)−Poly(butadiene) Diblock Copolymers: Evolution of the Random Network Morphology

**Sumeet Jain, Mitchell H. E. Dyrdahl, Xiaobo Gong, L. E. Scriven, and Frank S. Bates***

*Department of Chemical Engineering and Materials Science, University of Minnesota, Minneapolis, Minnesota 55455*

*Received October 18, 2007; Revised Manuscript Received February 26, 2008*

ABSTRACT: The phase behavior of poly(ethylene oxide)−poly(butadiene) (PEO-PB) diblock copolymers mixed with water was studied using small-angle X-ray scattering (SAXS), cryogenic scanning electron microscopy (cryo-SEM), cryogenic transmission electron microscopy (cryo-TEM), and dynamic mechanical spectroscopy. Two sets of diblocks were synthesized by adding different lengths of PEO to hydroxy terminated PB with degrees of polymerization $N_{PB} = 46$ and 170. Two-component mixtures were investigated as a function of block composition and copolymer molecular weight, between 1 and 100 wt % polymer content. Melt phase behavior is consistent with established theory and known experimental behavior for diblock copolymers. Various lyotropic liquid crystalline structures, notably lamellae (L), hexagonally packed cylinders (H), and spheres (S) arranged on cubic (body-centered cubic, face-centered cubic) lattices, were documented as a function of water content. At the higher molecular weights ($N_{PB} = 170$), a random network phase (N) was identified over a sizable portion of the phase portrait, located between hexagonally ordered cylinders and ordered lamellae. This new structure, along with branching of cylindrical micelles in the dilute limit, bear a striking similarity to experimentally observed and theoretically predicted phase behavior in certain ternary water/oil/surfactant systems. These findings demonstrate that block copolymer surfactants are characterized by at least four structural building blocks—spheres, cylinders, bilayers, and branched cylinders—above a threshold molecular weight.

## 1. Introduction

Self-assembly of amphiphilic molecules, such as surfactants and lipids, can produce a complex array of supramolecular structures. Dilute dispersions of surfactants have found uses as foaming agents, emulsifiers, wetting agents and compatibilizers and have been used in biomedical applications.[1] Mixing amphiphiles with an individual solvent (binary system) or a combination of solvents (e.g., ternary system) often leads to an array of disordered micelles at low concentrations and a host of lyotropic liquid crystalline (LLC) phases at higher concentrations, where the resulting morphology depends sensitively on the overall composition.

Relative to conventional surfactants, polymeric surfactants, such as poly(ethylene oxide-*b*-butadiene) (PEO-PB), offer some significant advantages, including continuously tunable chemical structures, larger domain dimensions that permit chemical modification such as cross-linking,[2,3] and incorporation of other desirable physical properties.[4] In the pure state, diblock copolymers self-assemble into four ordered structures: lamellae, cylinders, spheres, and an ordered bicontinuous network known as the gyroid. Self-assembly of diblock copolymers follows a universal phase diagram when described in terms of the segregation strength between blocks, proportional to the product $\chi N$, and the volume fraction of one of the blocks $f$,[5] where $\chi$ and $N$ are the Flory–Huggins parameter and overall degree of polymerization, respectively. Also, the morphology can be controlled by addition of a second component (usually a selective solvent) that swells one of the polymer domains, leading to materials with adjustable periodicities and microstructures. Over the past decade, many reports have described the structure and applications of such block copolymer lyotropic phases.[6] These materials have found applications in biomedical devices[7] and in the structural design of nanomaterials such as photonic crystals,[8] mesoporous media,[9] semiconductors,[10] arrayed metal nanoparticles[11] and polymer gels.[12]

Early studies with block copolymer mesophases, which exploited hydrocarbon-based materials such as poly(styrene-*b*-isoprene) (PS-PI) block copolymers, revealed that the solution behavior in selective organic solvents was only weakly analogous to conventional water-based amphiphilic systems.[13,14] For water-compatible polymers, most research efforts have focused on commercially available diblock and triblock copolymers containing poly(ethylene oxide) (PEO) and poly(propylene oxide) (PPO), known as Pluronics.[15–18] These industrial polymers have enjoyed commercial successes for nearly half of a century, although ambiguity in obtaining reproducible experimental results between different synthetic batches has been noted, for example, the phase diagram for "L122" ($E_{11}P_{70}E_{11}$) reported in two separate studies[16,19] is noticeably different.

In a comprehensive effort, Wanka et al.[15,16] studied 19 commercial PEO-PPO-PEO triblock copolymers and found that the lyotropic phase behavior was strongly dependent on the copolymer composition. They reported a sequence of mesophases (isotropic micellar solution (M), cubic phase (I), hexagonal phase (H), and lamellar phase (L)) that closely mimics what is found with surfactants. Alexandridis et al.[17] examined the composition, molecular weight, and temperature dependence of three pluronic polymers and found that the lyotropic phase behavior of these block copolymers also is weakly thermotropic, presumably owing to the lower critical solution temperature (LCST) behavior of PEO in water. Small-angle X-ray scattering (SAXS) experiments by McConnell et al.[20] and Hamley et al.[21] revealed that copolymers with short hydrophilic blocks order into face-centered cubic (FCC) crystals, whereas copolymers with long hydrophilic blocks form body-centered cubic (BCC) arrays.

Synthetic advances in the past decade have simplified the preparation and investigation of amphiphilic block copolymers containing hydrophilic segments such as PEO and poly(acrylic acid).[22–26] Nonionic macromolecular surfactants containing a hydrocarbon block (e.g., PB-PEO), poly(isoprene-*b*-ethylene oxide) (PI-PEO), and poly(styrene-*b*-ethylene oxide) (PS-PEO)) can be synthesized using anionic polymerization. Chemically,

* Corresponding author e-mail: bates@cems.umn.edu.

10.1021/ma702322b CCC: $40.75 
Published on Web 04/12/2008

these block copolymers resemble the generic nonionic $C_iE_j$-type surfactants and, hence, represent an attractive model system for comparing the aggregation behavior of polymeric and low molecular weight surfactants. Low glass transition temperatures for PB and PI blocks ($T_g < -10$ °C) permit unencumbered chain movement facilitating efficient dispersion of the copolymers in water at all concentrations and at ambient temperature. Moreover, poly(diene) blocks can be cross-linked, resulting in the enhancement of certain physical properties;[6,27–29] cross-linking self-assembled lipids and oligomeric surfactants usually disrupts the targeted morphology.[30]

Aqueous mixtures of nearly symmetric PEO-PB diblock copolymers were characterized by Förster et al.[6] using polarized light optical microscopy and transmission electron microscopy. They observed a familiar set of structural transitions, from disordered spherical micelles (M), to spheres ordered on a BCC lattice (BCC), to hexagonally packed cylinders (H), and finally, to lamellae (L) as the polymer concentration increased. Hentze et al.[27] used PEO-PB to template mesoporous silica. A PEO-PI diblock copolymer with $f_{PEO} = 0.64$ was shown by Messe et al.[28] to exhibit the sequence of phases M-I-L, with decreasing water content; curiously, the hexagonal phase (H) is conspicuously absent.

Recent years have witnessed the development of more complex amphiphilic block copolymer architectures that target more sophisticated applications. For example, Förster and coworkers have designed pH responsive vesicles using P2VP-PEO diblock copolymers.[31] In another example, Stoenescu and Meier[32] report vesicle formation from a poly(ethylene oxide-b-dimethylsiloxane-2-methyloxazoline) (PEO-PDMS-PMOXA) triblock copolymer. A comprehensive survey of the literature dealing with amphiphilic block copolymers is beyond the scope of this article.

Network structures with interconnected domains have attracted scientific attention for many years because they provide tantalizing opportunities for the design of materials with controllable mechanical, transport, and optical properties. Porous, bicontinuous, materials with well-defined pore sizes have generated technological interest, based on applications in aerogels,[33] membranes,[34] and low-density materials.[6,9] Several protocols, including spinodal decomposition,[35] etching, nucleation and growth, and self-assembly,[27] have been employed to create these materials. Network morphologies based on binary and ternary mixtures containing amphiphilic compounds have been proposed theoretically[36,37] and realized in practice.[38,39] A variety of fascinating bicontinuous morphologies, including the sponge-phase,[40] double-diamond,[41] hexagonally perforated lamellae,[42] and gyroid,[43] have been reported in solvated surfactant systems. A few publications have documented bicontinuous cubic morphologies in binary and ternary systems containing block copolymers.[44]

Motivated by our earlier success in characterizing the effects of molecular weight[45] and slow chain dynamics on the micellization of block copolymer surfactants,[46] we have extended this work to include higher concentrations of PB-PEO diblock copolymer, extending from the melt down to a state of dispersion. Ryan and co-workers have provided an array of insightful publications dealing with this subject, beginning with an article that describes the phase behavior of undiluted poly(ethylene oxide-*b*-butylene oxide) (PEO-PBO) diblock copolymers.[47] Subsequently, they investigated this model system by small-angle X-ray and neutron scattering as a function of concentration in water and temperature, under quiescent and flowing conditions.[48] More recently, Battaglia and Ryan[49–52] have addressed the issue of bulk, and concentrated, PEO-PBO hydration, particularly with respect to vesicle formation. These authors have shown that transforming neat block copolymer into micelles or vesicles is fraught with complexity, leading to unusual morphological features such as tubular membranes, and dramatic changes in viscoelastic behavior.

The work reported here targets more modest goals, specifically, to establish whether micellar branching, documented in the dilute regime,[45] is manifested at intermediate block copolymer concentrations in water. A preliminary letter based on a single set of homologous specimens (i.e., containing a common PB molecular weight) showed the existence of a disordered network phase over a wide range of PEO compositions and concentrations.[53] This article adds a complementary phase diagram obtained with a homologous set of lower molecular weight PB-PEO.

Fourteen PEO-PB diblock copolymers, derived from two PB precursor polymers (PB degree of polymerization $N_{PB} = 46$ and 170), with different compositions and formulated with varying amounts of water, have been investigated. SAXS, cryogenic scanning electron microscopy (cryo-SEM), cryogenic transmission electron microscopy (cryo-TEM), and dynamic mechanical spectroscopy techniques have been employed to characterize these mixtures. This effort has revealed that the random network morphology (denoted N) formed from interconnected struts with predominately cylindrical symmetry, situated at concentrations and compositions between those associated with hexagonal and lamellar phases, disappears as the molecular weight is reduced. Remarkably, Tlusty et al.[54] and Hyde et al.[37] have anticipated the sequence of topological transitions that we document at higher molecular weight for conventional three-component (surfactant/oil/water) microemulsions. These findings suggest that cylinder branching and network formation may be a universal feature of self-assembling amphiphilic systems.

## 2. Experimental Section

**2.1. Materials.** A two-step living anionic polymerization technique was employed to synthesize poly(ethylene oxide-*b*-butadiene) (OB) diblock copolymers.[22] Sizeable batches (~120 g) of 1,3-butadiene (Aldrich) were polymerized using *sec*-butyl lithium initiator in tetrahydrofuran (THF) forming poly(1,2-butadiene), which was subsequently end-capped using ethylene oxide and followed by termination with acidic (HCl) methanol to form hydroxyl-terminated poly(butadiene). Small quantities (~5 g) of hydroxyl-terminated poly(butadiene) were reinitiated in purified THF using potassium napthalenide, followed by addition of quantitative amounts of ethylene oxide and termination with acidic methanol, to obtain OB diblock copolymers. This two-step synthesis scheme is particularly suited for this study because families of diblock copolymers containing identical hydrophobic blocks (B), but varying hydrophilic (PEO) content, can be prepared.

Polydispersity indices (PDIs) were determined by gel permeation chromatography (GPC), using a Waters 150C instrument fitted with Phenogel columns (10 000, 5000 and 500 Å pore size). Measurements were done at 25 °C with THF as the mobile phase, and the columns were calibrated with poly(styrene) standards (Pressure Chemical Co.). In all cases, GPC traces were characterized by a single, monomodal peak, indicative of the efficient reinitiation of hydroxy-poly(butadiene), and the absence of homopolymer in the diblock product. Diblock copolymer molecular weights ($M_n$) and compositions (weight fraction of PEO, $w_{PEO}$) were determined from the reaction stoichiometry and $^1$H NMR spectroscopy, using a Varian 300 MHz instrument, with all samples dissolved in deuterated chloroform. Proton ($^1$H)-NMR spectroscopy also was employed to determine the PB microstructure (90% 1,2-addition). Two series of OB diblock copolymers with different core number average degrees of polymerization ($N_{PB}$) and varying hydrophilic PEO block lengths were synthesized. For the OB1 series, diblock copolymers with $0.30 \leq w_{PEO} \leq 0.64$ ($1.03 < PDI < 1.06$) and a core molecular weight of 2500 g/mol ($N_{PB} = 46$) were synthesized. Another set of diblock copolymers, the OB9 series, was synthesized

**Table 1. Molecular Characteristics of Block Copolymers**

| ID[a] | $M_n$ (kg/mol)[b] | $N_{PB}$[c] | $N_{PEO}$[d] | $w_{PEO}$[e] | $T_{ODT}$[f] | PDI[g] | micelle structure[h] |
|---|---|---|---|---|---|---|---|
| OB1–11 | 3.4 | 46 | 24 | 0.30 | 83 °C | 1.03 | B |
| OB1–2 | 3.5 | 46 | 28 | 0.32 | 87 °C | 1.05 | B |
| OB1–10 | 3.7 | 46 | 30 | 0.34 | 90 °C | 1.06 | B |
| OB1–9 | 3.9 | 46 | 35 | 0.37 | 105 °C | 1.04 | B, C |
| OB1–15 | 4.1 | 46 | 39 | 0.40 | 113 °C | 1.04 | B, C |
| OB1–5 | 4.3 | 46 | 42 | 0.42 | 117 °C | 1.04 | B, C |
| OB1–1 | 4.4 | 46 | 50 | 0.46 | 120 °C | 1.04 | C, B |
| OB1–8 | 5.0 | 46 | 56 | 0.49 | 139 °C | 1.03 | C |
| OB1–3 | 5.2 | 46 | 58 | 0.50 | 156 °C | 1.05 | C, S |
| OB1–14 | 5.3 | 46 | 60 | 0.51 | 159 °C | 1.04 | C |
| OB1–13 | 5.4 | 46 | 63 | 0.52 | 162 °C | 1.04 | C |
| OB1–6 | 5.8 | 46 | 69 | 0.54 | 170 °C | 1.03 | C, S |
| OB1–7 | 7.0 | 46 | 93 | 0.62 | 195 °C | 1.04 | S, C |
| OB1–4 | 7.6 | 46 | 103 | 0.64 | 198 °C | 1.04 | S |
| OB9–6 | 12.1 | 170 | 66 | 0.24 | >200 °C | 1.04 | B |
| OB9–15 | 13.2 | 170 | 90 | 0.30 | >200 °C | 1.06 | B, $C_Y$ |
| OB9–4 | 14.0 | 170 | 110 | 0.34 | >200 °C | 1.04 | N |
| OB9–11 | 15.1 | 170 | 134 | 0.39 | >200 °C | 1.04 | $C_Y$ |
| OB9–1 | 15.8 | 170 | 150 | 0.42 | >200 °C | 1.04 | C |
| OB9–9 | 16.1 | 170 | 158 | 0.43 | >200 °C | 1.04 | C, S |
| OB9–10 | 16.0 | 170 | 156 | 0.43 | >200 °C | 1.10 | C, S |
| OB9–2 | 16.4 | 170 | 164 | 0.44 | >200 °C | 1.05 | C, S |
| OB9–5 | 18.1 | 170 | 203 | 0.49 | >200 °C | 1.05 | S, C |
| OB9–3 | 19.0 | 170 | 225 | 0.51 | >200 °C | 1.06 | S, C |
| OB9–7 | 19.3 | 170 | 231 | 0.52 | >200 °C | 1.04 | S, C |
| OB9–13 | 24.2 | 170 | 341 | 0.62 | >200 °C | 1.08 | S |
| OB9–12 | 30.2 | 170 | 478 | 0.70 | >200 °C | 1.09 | S |

[a] Diblock copolymers of poly(ethylene oxide) (PEO) and poly(butadiene) (PB). [b] Number-average molecular weight determined from reaction stoichiometry and $^1$H NMR. [c] Number of monomer repeat units in the PB block. [d] Number of monomer repeat units in the PEO block. [e] Weight fraction of the PEO block in the diblock copolymer. [f] Order–disorder transition temperature measured from dynamic mechanical analysis. [g] Polydispersity index determined from gel permeation chromatography. [h] Morphologies formed in 1 wt% dispersions in and identified by cryo-TEM: B = bilayers; C = cylinders, S = spheres, N = network, $C_Y$ = cylinders with Y-junctions. Coexisting structures are written in order of statistical predominance.

with a core molecular weight of 9200 g/mol ($N_{PB} = 170$) and $0.24 \leq w_{PEO} \leq 0.70$ ($1.04 < \text{PDI} < 1.10$). Molecular details of the diblock copolymers are listed in Table 1.

**2.2. Small Angle X-ray Scattering.** Samples for scattering measurements were prepared by dissolution of measured amounts of diblock copolymer in methylene chloride in a glass vial. The samples were then slowly dried, leaving behind a thin film of copolymer along the walls of the vial. Subsequently, defined amounts of high-purity water (HPLC grade) were added, and the sample vials were capped and sealed using laboratory film (Parafilm). Samples were then stirred and centrifuged at room temperature for a week. Initial mixing was followed by homogenization through repeated cycles of stirring, centrifugation, annealing at a moderate temperatures (ca. 40 °C), and thermal cycling across the melting point of the PEO block for a period of six weeks, to facilitate complete dispersion. There was no appreciable loss of water as estimated from sample weight measurements at regular intervals during the homogenization process. Samples with polymer concentration less than 25% were transferred to quartz capillaries, 1.5 mm in outer diameter, which were then sealed with commercial epoxy (Loctite Quick-set epoxy). Melt and concentrated samples were sandwiched between Kapton windows separated by an O-ring just prior to measurement. This protocol minimizes the loss of water. Multiple measurements were performed with the concentrated samples to ensure reliability and reproducibility of the results. Morphological assignments were made on the basis of the diffraction peaks that occur at specific wavevector ratios.

SAXS measurements were conducted on the DND-CAT at the Advanced Photon Source at Argonne National Laboratory and using beamlines maintained at the University of Minnesota. The data for melt samples was collected at temperatures between 25 and 200 °C. Dilute and intermediate concentration samples (in capillaries) were investigated at 25, 40, and 60 °C; only the 25 °C results are reported here. The limited range of temperatures was employed in order to minimize water loss and to avoid seal failure. No morphology changes were recorded over this temperature range. (Although the domain spacing decreases slightly upon heating, this change was insignificant compared to the variations in domain spacing encountered upon changing the concentration). All melt sample scattering data reported here was acquired at 80 °C.

**2.3. Cryo-TEM.** Sample solutions for cryo-TEM were prepared by direct dissolution of diblock copolymers in high purity water (HPLC grade) at a concentration of 1 wt %. The samples were sealed and stirred at room temperature for a minimum of two weeks. Most polymers dispersed in water in a couple of hours, except those with the highest poly(butadiene) content, which took a few days. All of the polymer solutions discussed here appeared homogeneous to the naked eye, although they were characterized by varying degrees of opacity.

Samples were vitrified for morphological studies using a custom-built chamber referred to as the controlled-environment vitrification system (CEVS).[55] To prevent appreciable loss of water from the sample solutions, the CEVS chamber was humidified to saturation at 25 ± 0.2 °C. Cryo-TEM samples were prepared by placing with a pipet a drop (~5 μL) of solution onto a copper grid, held by tweezers. Excess solution was blotted using a piece of filter paper, resulting in the formation of a thin film, about 100–300 nm thick, held by capillary forces within the holes of a lacey carbon film supported on the metal grid. After blotting, the samples were held at ambient temperature for approximately 30 s to relax residual stresses. The sample grids were then quickly plunged into a reservoir of liquid ethane cooled by liquid nitrogen. Vitrified samples were temporarily stored in liquid nitrogen prior to loading on the cryogenic sample holder (Gatan 626). Vitrified specimens were examined with a JEOL 1210 TEM operated at 120 kV. A minimal dose system was employed to avoid sample damage by radiolysis.[56] Adequate phase contrast was obtained at a nominal underfocus of about 3−12 μm. Images were recorded on a Gatan 724 multiscan digital camera and were processed with DigitalMicrographs ver. 3.3.1. Ramp-shaped optical density gradients, present as a background due to varying sample thickness, were digitally corrected. Diffraction grating replicas (Ted-Pella) containing 2160 lines per millimeter were used to calibrate the microscope.

**2.4. Cryo-SEM.** Cryo-SEM studies were conducted on concentrated copolymer samples identical or equivalent to the samples prepared for SAXS measurements. The highly viscous samples were smeared into two "freezing hats" each about 100 μm deep, which were carefully angled together to exclude air. The assemblage was loaded into a Bal-Tec HPM 010 high-pressure freezing machine (Balzers, Lichtenstein), quickly pressured to 2100 bar, and rapidly cooled (~10 ms) by jets of liquid nitrogen. The high pressure lowers the supercooling limit of water and greatly elevates its viscosity (already high at atmospheric pressure in the concentrated PEO-PB samples), thereby yielding fast-frozen samples with negligible freezing artifacts. The sample assembly was transferred into a liquid nitrogen bath where it was pried open to fracture the sample longitudinally. One side was mounted in a Gatan 626 cryo-transfer stage (Gatan, Pleasanton, CA) and transferred into a precooled Balzers MED 010 freeze-drying and sputtering device (Balzers Union, Balzers, Lichtenstein) against a counterflow of cold dry nitrogen gas. Vitrified water in and immediately below the fracture surface was partially sublimed away at −96 °C and approximately $2 \times 10^{-9}$ bar for about 9 min to expose the less volatile structure while avoiding recrystallization of the remaining vitrified water. The exposed surface topography was coated at −130 °C with a conducting deposit of platinum, nominally 2–3 nm thick. The coated sample was then transferred at −150 °C into a Hitachi S900 in-the-lens field emission scanning electron microscope, maintained at about −170 °C, and examined at a low acceleration voltage of 3 keV to avoid excessive charging and radiation damage of the areas imaged.

**2.5. Dynamic Mechanical Spectroscopy (DMS).** Mechanical spectroscopy experiments were conducted on a Rheometric Sci-

entific ARES strain-controlled rheometer using a parallel plate configuration with 25 mm diameter plates. Isochronal ($\omega = 1$ rad/s) temperature ramps at a constant heating rate (2 °C/min) were conducted to measure the dynamic elastic ($G'$) and loss ($G''$) moduli. The experiments were run in a nitrogen filled chamber to minimize sample oxidation at elevated temperatures. A strain amplitude of 1% was chosen such that all isochronal temperature ramp measurements were conducted in the linear viscoelastic region. Order–disorder transition temperatures ($T_{ODT}$) were associated with an abrupt decrease in the dynamic elastic modulus during heating. The frequency dependence of $G'$ and $G''$ was probed for the concentrated samples by dynamic frequency sweeps from 0.05 to 100 rad/s at strain amplitudes of less than 20% on a strain-controlled Rheometrics fluid spectrometer (RFS-II). This instrument has a torque range of 0.002−100 g•cm with an accuracy of 1%. The linear viscoelastic regime (that is, the region where the rheological response is independent of the strain amplitude) was determined by dynamic strain sweep measurements.

## 3. Results and Analysis

We have characterized the phase behavior of aqueous mixtures of the OB1 ($N_{PB} = 46$) and OB9 ($N_{PB} = 170$) diblock copolymers. SAXS, microscopy (cryo-TEM and cryo-SEM), and dynamic mechanical spectroscopy were employed for this purpose. Selected experimental results are presented and evaluated in this section. Our analysis has resulted in two comprehensive phase maps that establish a distinct molecular weight dependence to block copolymer self-assembly in the presence of water, along with a new morphology at the higher molecular weight.

**3.1. Melt Phase Behavior.** SAXS data collected from the OB diblock copolymers at temperatures below the melting temperature of PEO ($T_m = 55$ °C) displayed broad reflections due to PEO crystallinity, which distorts the state of local order (not shown). Above 55 °C, these materials develop well-defined microstructures with long-range order. Order–disorder transition temperatures ($T_{ODT}$) were identified using $G'$ measurements recorded as a function of temperature while heating (2 °C/min) OB1 specimens between 25 and 200 °C; this technique is described elsewhere.[57] All the copolymers in the low molecular weight (OB1) series exhibit an ODT upon heating, with transition temperatures ($T_{ODT}$) ranging from 83 to 198 °C, that is, $T_{ODT}$ increases with increasing PEO content (Table 1). No such transitions were detected for the high molecular weight block copolymers (OB9 series) in the temperature range studied (25 °C < $T$ < 200 °C), indicative of inaccessibly high $T_{ODT}$ values.

The melt phase behavior of the OB1 and OB9 diblock copolymers was investigated using SAXS. Powder patterns were recorded with Bragg reflections at ratios of peak positions $q/q^*$ ($q^*$ is the location of the first-order peak) of 1:2:3:4:5:6:7, $\sqrt{6}$:$\sqrt{8}$, 1:$\sqrt{3}$:$\sqrt{4}$:$\sqrt{7}$:$\sqrt{9}$:$\sqrt{12}$:$\sqrt{13}$:$\sqrt{16}$, and $\sqrt{2}$:$\sqrt{4}$:$\sqrt{6}$:$\sqrt{8}$:$\sqrt{10}$:$\sqrt{12}$:$\sqrt{14}$. These are associated with ordered lamellar (L), gyroid (G), hexagonally packed cylinders (H), and BCC packed spherical morphologies, respectively. A more comprehensive discussion of the methods employed can be found elsewhere.[58] For cylinders arranged on a hexagonal lattice, we have adopted the notation H, instead of the commonly used C notation, for cylinders. The hexagonal packing of cylinders can be further divided into $H_1$ and $H_2$ denoting "normal" (subscript 1, PB structures in a PEO matrix) and "inverse" (subscript 2, PEO structures in a PB matrix), respectively. Similarly, the gyroid is denoted as either $G_1$ or $G_2$. Because scattering cannot differentiate between "normal" and "inverse" morphologies, assignments were assumed based on the block copolymer composition, relative to the location of lamellae.

**3.2. Dilute Dispersions.** Self-assembly of OB1 and OB9 diblock copolymers in dilute aqueous solution was described in an earlier report.[46] The following morphologies were identified in 1 wt % dispersions with increasing PEO weight fraction ($w_{PEO}$) in the PEO-PB diblocks: vesicles (B), worm-like cylindrical micelles (C), branched cylindrical micelles ($C_Y$), a two-phase state that contains a three-dimensional network (N) structure, and spherical micelles (S). Mixed morphologies (e.g., B + C) were found over sizable regions of this parameter space. Similar morphological correlations have been reported in earlier studies dealing with diblock copolymer dispersions.[59,60]

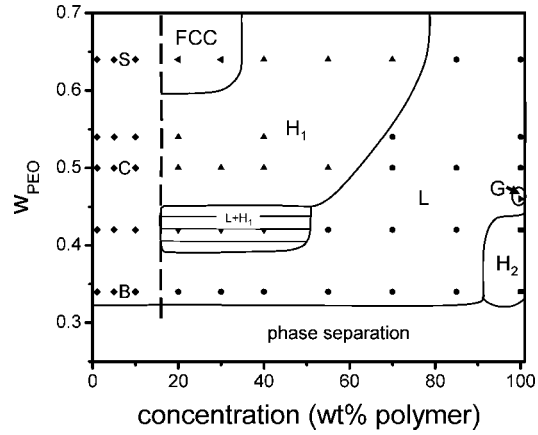


**Figure 1.** Experimental phase portrait for the OB1 series of diblock copolymers in water. Structures are identified as a function of $w_{PEO}$ and the concentration of copolymer in solution (by wt %). Solid lines mark approximate phase boundaries, and thin horizontal lines identify coexistence regions. The following ordered structures are present: cylinders of PEO/water arranged on a hexagonal lattice ($H_2$, ■); gyroid (G); lamellae (L, ●); coexistence of lamellae and hexagonal (L + $H_1$, ▼); PB cylinders ($H_1$, ▲); and spheres (FCC, "solid left triangle"). Upon dilution, three disordered micellar morphologies occur: bilayers (B) vesicles, cylinders (C), and spheres (S), as identified by cryo-TEM.[46] At low $w_{PEO}$ values, the OB1 block copolymers are not dispersible in water.

Increasing the core molecular weight 4-fold ($N_{PB} = 170$, OB9 series), results in the emergence of branched structures at compositions intermediate to those associated with bilayers and cylinders.[45] Decreasing the PEO content from the cylindrical regime results in cylinders with Y-junctions (denoted $C_Y$). Branching density peaks at a composition midway between the cylinder and bilayer regions, resulting in the formation of the phase separated network (N), or highly reticulated network fragments following vigorous agitation.[45] Although occasional branching was recorded with the low molecular weight copolymer solutions, network formation and macroscopic phase separation in the dilute limit (1%) was only found in the high molecular weight copolymer dispersions. Aside from this branching phenomenon, the morphological properties of the OB9 series of diblock copolymers parallel those of the OB1-series, with modest shifts in the molecular compositions where transitions between structures occur.

**3.3. Intermediate Concentrations.** To facilitate our presentation and analysis of a large amount of experimental data obtained at intermediate concentrations (5% ≤ wt % ≤ 90%), we first individually summarize the phase behavior of the OB1 and OB9 mixtures, followed by a description of the experimental basis for the phase assignments. Here we note that these depictions are not proper phase diagrams because the ordinate reflects changes in chemical structure. Hence, we refer to these illustrations as either "phase portraits" or "phase maps".

*3.3.1. OB1 ($N_B = 46$).* Figure 1 identifies the phase behavior at room temperature (80 °C for the bulk polymers) obtained from five sets of aqueous mixtures (OB1–1, OB1–5, OB1–3, OB1–6, and OB1–4) with compositions ($w_{PEO}$) ranging from 0.34 to 0.64. Ten samples were prepared for each of the these diblocks (except seven for OB1–6) by mixing 1, 5, 10, 20, 30,

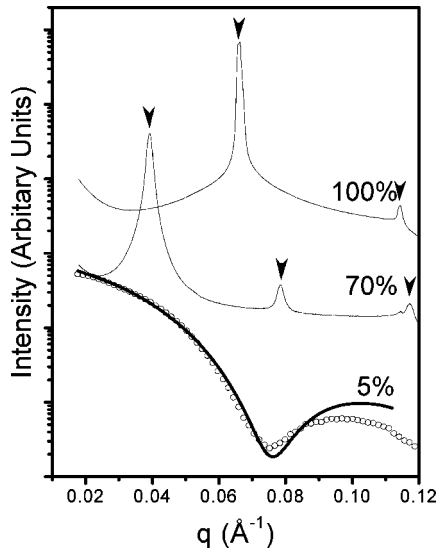


**Figure 2.** SAXS patterns obtained from OB1–10 ($w_{PEO} = 0.35$) as a function of copolymer concentration. Inverted arrows mark the calculated positions of diffraction peaks for the assigned morphology: 100% ($\sqrt{1}$:$\sqrt{3}$, hexagonal, $H_2$); 70% (1:2:3, lamellar, L), 5% (disordered bilayer vesicles, B).

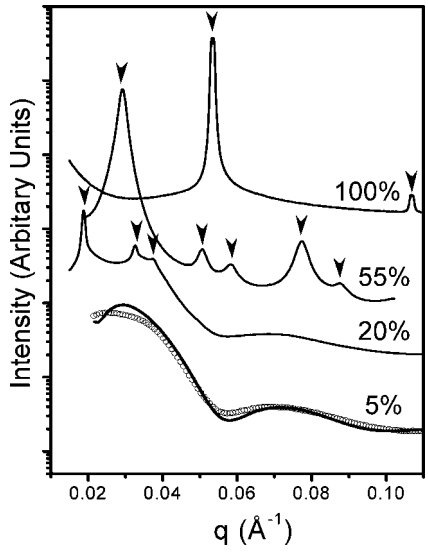


**Figure 3.** SAXS patterns obtained from OB1–3 ($w_{PEO} = 0.50$) as a function of copolymer concentration. Relative peak positions and assigned morphologies: 100% (1:2, lamellar, L); 55% ($\sqrt{1}$:$\sqrt{3}$:$\sqrt{4}$:$\sqrt{7}$:$\sqrt{9}$, hexagonal, $H_1$); 20% ($\sqrt{1}$:$\sqrt{3}$:$\sqrt{4}$, hexagonal, $H_1$); 5% (disordered cylinders, C).

40, 55, 70, 85, and 100 wt % copolymer with water. The dilute (1 wt %) and melt (100 wt %) behavior have been considered in the previous sections. The addition of water to these amphiphilic materials leads to several ordered states (L, $H_1$, and FCC) above about 15 wt % block copolymer, three disordered dispersions (S, C, and B) below about 15 wt %, and multiphase (L + $H_1$) and macroscopic phase separation (insoluble for $w_{PEO} < 0.34$) as indicated.

Representative SAXS results, selected from an extensive amount of data, are presented in Figures 2−4, representing copolymer solutions derived from OB1–4, OB1–3, and OB1–10, respectively, which form spheres, cylinders, and vesicles in the dilute limit, respectively. Each illustration includes the melt SAXS data for easy comparison with the solution results.

Three distinct phases are identified for OB1–10 ($w_{PEO} = 0.34$) in Figure 1: $H_2$ in the melt (see above), L between 20 and 85

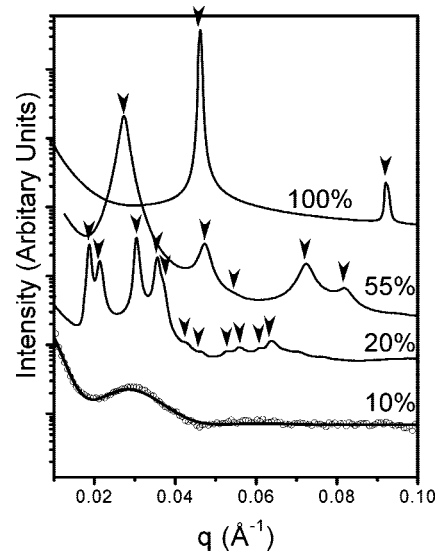


**Figure 4.** SAXS patterns obtained from OB1–4 ($w_{PEO} = 0.64$) as a function of copolymer concentration. Relative peak positions and assigned morphologies for 100% (1:2, Lamellar, L); 55% ($\sqrt{1}$:$\sqrt{3}$:$\sqrt{7}$:$\sqrt{9}$, hexagonal, $H_1$); 20% ($\sqrt{3}$:$\sqrt{4}$:$\sqrt{8}$:$\sqrt{11}$:$\sqrt{12}$:$\sqrt{16}$:$\sqrt{19}$:$\sqrt{24}$:$\sqrt{27}$:$\sqrt{35}$, FCC); 10% (disordered spheres, S).

wt %, and dispersed vesicles (B) at and below 10 wt % block copolymer. The SAXS powder pattern for the 70 wt % specimen (Figure 2), which contains peaks at relative positions 1:2:3, supports a lamellar morphology (L); similar results were obtained from all OB1 based specimens identified as L in Figure 1. Scattering data obtained from milky dilute solutions containing less than 15 wt % OB1–10 were devoid of Bragg diffraction but contain features consistent with form factor scattering (Figure 2; 5 wt %). On the basis of the vesicle morphology (B) obtained in the dilute limit (cryo-TEM, not shown), we have modeled this SAXS profile using a hollow sphere geometry with a membrane core thickness $L = 6.8$ nm, and $\Delta L/L = 0.13$, as shown by the solid curve.[61,62] This representation captures the general features of the scattering pattern, reinforcing the vesicle bilayer (B) assignment.

SAXS measurements from several OB1–3 ($w_{PEO} = 0.50$) mixtures are shown in Figure 3. Bulk OB1–3 has a lamellar morphology (see above), which persists with the addition of water up to a concentration of 70 wt % copolymer. At 55 wt % a new pattern emerges, with relative peak positions at $\sqrt{1}$:$\sqrt{3}$:$\sqrt{4}$:$\sqrt{7}$:$\sqrt{9}$, consistent with hexagonally packed cylinders ($H_1$). Additional water swells the $H_1$ structure, which persists down to 20 wt % copolymer; at this concentration the scattering trace contains fewer peaks ($\sqrt{1}$:$\sqrt{3}$:$\sqrt{4}$), making the form factor scattering at higher $q$-values more evident, suggestive of shorter range order. At and below10 wt % copolymer, only form factor scattering was recorded, indicative of an isotropic dispersion. On the basis of the identification of cylindrical micelles (C) in the dilute limit (cryo-TEM, not shown), we have modeled the 5 wt % OB1–3 SAXS pattern using a cylindrical form factor,[61] with core radius $R_C = 7.0$ nm, and $\Delta R_C/R_C = 0.12$. This model closely accounts for the experimental data.

The final set of examples for the OB1 specimens are presented in Figure 4. Addition of water to OB1–4 ($w_{PEO} = 0.64$) transforms the bulk L phase (see above) to the $H_1$ state between 40 and 70 wt % copolymer, as demonstrated by the SAXS pattern obtained from the 55 wt % specimen (peaks located at $\sqrt{1}$:$\sqrt{3}$:($\sqrt{4}$):$\sqrt{7}$:$\sqrt{9}$). Further dilutions, to 30 and 20 wt %, lead to a new state of ordering, with peaks situated at $\sqrt{3}$:$\sqrt{8}$:$\sqrt{12}$:$\sqrt{19}$:$\sqrt{24}$:$\sqrt{27}$:$\sqrt{35}$. This pattern is uniquely associated with an FCC lattice, to which we ascribe a spherical morphology. At and below 10 wt % the solutions become disordered,

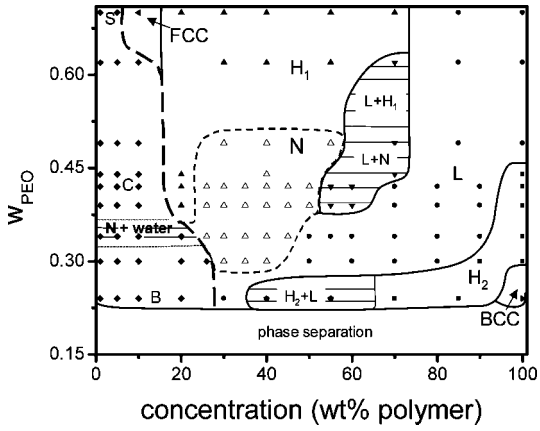


**Figure 5.** Experimental phase portrait for the OB9 series of diblock copolymers in water. Structures are identified as a function of the composition of diblock copolymer ($w_{PEO}$) and the concentration of copolymer in solution (by wt %). Solid lines mark approximate phase boundaries, and thin horizontal lines identify coexistence regions. The following ordered structures are present: spheres of PEO packed with body-centered symmetry in a PB matrix (BCC, "solid left triangle"); cylinders ($H_2$, ■); lamellae (L, ●); cylinders of PB packed on a hexagonal lattice in a PEO/water matrix ($H_1$, ▲); spheres (FCC, "solid left triangle"). A disordered network morphology is denoted by (N, Δ). Two phase coexistence regions (L + $H_1$ and L + N, ▼) separate single phase regions. Upon dilution, the ordered structures disintegrate into disordered micelles (S, C) and bilayer vesicles (B), as delineated by the long-dashed line. At low $w_{PEO}$ values OB9 copolymers are not dispersible in water. Reproduced from ref 53.

producing only form factor scattering, which we have modeled using a hard sphere form factor[61] with core radius $R_S = 9.1$ nm and $\Delta R_S/R_S = 0.14$ (solid curve). Cryo-TEM images obtained in the dilute (1 wt %) limit (not shown) are consistent with this result.

Coexistence of L and $H_1$, identified in Figure 1, was established by indexing two sets of diffraction peaks in a single SAXS pattern. These results are omitted for brevity.

*3.3.2. OB9 ($N_B$ = 170). 3.3.2.1. SAXS.* Between 7 and 16 aqueous solutions, containing different amounts of water, were examined for each of 9 specimens from the family of OB9 diblock copolymers listed in Table 1 (OB9–6, OB9–15, OB9–4, OB9–11, OB9–1, OB9–2, OB9–5, OB9–13, and OB9–12). Figure 5 identifies the resulting phase map, which includes three dispersed (disordered) morphologies (S, C, B), four ordered phases (FCC, $H_1$, L, $H_2$), a new disordered network phase (N), two-phase regions (L + $H_1$, L + N, $H_2$ + L), and macroscopic phase separation (immiscibility). In this section we present and analyze representative SAXS data, drawn from a subset of polymer mixtures (OB9–12, OB9–11, OB9–6, and OB9–1), along with cryo-SEM images taken from various hydrated specimens, illustrating how these assignments were determined.

Figure 6 contains SAXS traces derived from mixtures of water and OB9–12 ($w_{PEO} = 0.70$). Addition of up to 20 wt % water swells the bulk lamellar structure, and an $H_1$ phase is found between 10 and 70 wt % block copolymer, as evidenced by several orders of appropriate diffraction. (For the 10 wt % mixture, the first-order peak occurs at about 0.0054 $Å^{-1}$, which corresponds to a (110) hexagonal spacing of 116 nm). Further dilution leads to disordered spherical micelles; the SAXS pattern is quantitatively accounted for by a spherical form factor with $R_S = 21.6$ nm and $\Delta R_S/R_S = 0.15$ as shown by the solid curve in Figure 6 (5% result).

At the other limit of our range of compositions, data from OB9–6 ($w_{PEO} = 0.24$) are presented in Figure 7. Here, dilution of the bulk (BCC spheres) material results first in a $H_2$ structure, as evidenced by the diffraction pattern for the 85 wt % specimen, which contains peaks at relative spacings of $\sqrt{1}:\sqrt{3}:\sqrt{7}:\sqrt{9}$.

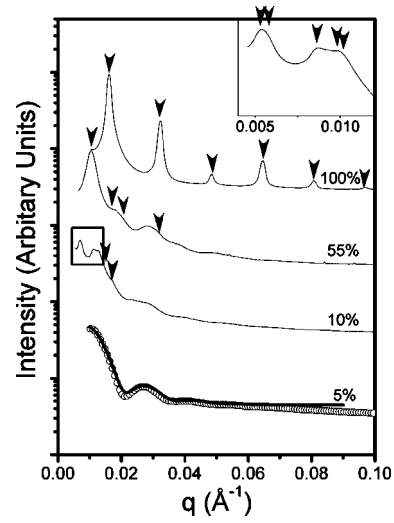


**Figure 6.** SAXS patterns obtained from OB9–12 ($w_{PEO} = 0.70$) copolymer as a function of copolymer concentration. Inverted arrows mark the calculated positions of diffraction peaks for the assigned morphology: 100% (1:2:3:4:5:6, lamellar, L); 55% ($\sqrt{1}:\sqrt{3}:\sqrt{7}:\sqrt{9}:\sqrt{13}$, hexagonal, $H_1$); 10% ($\sqrt{3}:\sqrt{4}:\sqrt{8}:\sqrt{11}:\sqrt{12}:\sqrt{19}$, FCC) (a selected area of the 10% trace is expanded in the inset); 5% (disordered spheres, S).

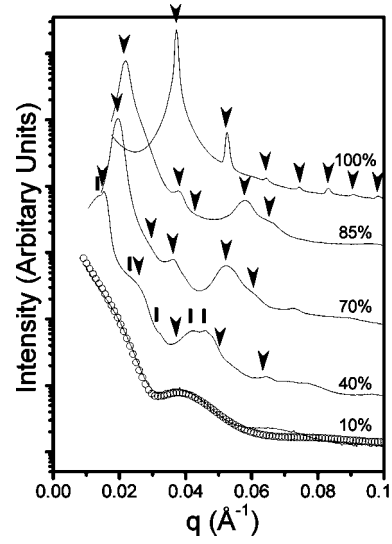


**Figure 7.** SAXS patterns obtained from OB9–6 ($w_{PEO} = 0.24$) copolymer as a function of copolymer concentration. Relative peak positions and assigned morphologies: 100% ($\sqrt{1}:\sqrt{2}:\sqrt{3}:\sqrt{4}:\sqrt{5}:\sqrt{6}:\sqrt{7}$, BCC), 85 and 70% ($\sqrt{1}:\sqrt{3}:\sqrt{4}:\sqrt{7}:\sqrt{9}$, hexagonal, $H_2$); 40% ($\sqrt{1}:\sqrt{3}:\sqrt{4}:\sqrt{9}:\sqrt{13}:\sqrt{16}:\sqrt{21}$ (vertical lines), and 1:2:3:4:5 (inverted arrows), hexagonal, $H_2$, and lamellar, L, respectively); 10% (disordered bilayer vesicles, B).

Absence of a $\sqrt{4}$ reflection likely results from form factor extinction. This point is reinforced by the scattering from the 70 wt % specimen, which contains peaks at $\sqrt{1}:\sqrt{4}:\sqrt{7}:\sqrt{9}:\sqrt{12}$. Thus, changing the composition (volume fraction of cylindrical cores) has shifted the extinction as expected. Reducing the amount of diblock copolymer to 40 wt % leads to a SAXS pattern that cannot be indexed with a single symmetry. However, assuming the presence of both $H_2$ and L phases, we are able to satisfactorily account for the peak intensities (including two principle reflections), and on this basis we have assigned a two-phase (L + $H_2$) state to this specimen and the one at 55 wt %. Finally, at concentrations of 20 wt % and lower, OB9–6 solutions were opaque, consistent with vesicle (B) formation, which was also confirmed in the dilute limit by cryo-TEM (not shown). Form-factor scattering was calculated

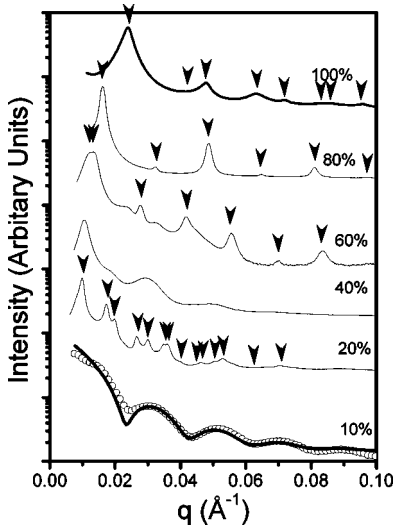


**Figure 8.** SAXS patterns obtained from OB9–1 ($w_{PEO}$ = 0.42) copolymer as a function of copolymer concentration. Relative peak positions and assigned morphologies: 100% ($\sqrt{1}$:$\sqrt{4}$:$\sqrt{7}$:$\sqrt{9}$:$\sqrt{12}$:$\sqrt{13}$:$\sqrt{16}$, hexagonal, $H_2$); 80% (1:2:3:4:5:6, Lamellar, L); 60% (1:2:3:4:5:6 (inverted triangles), lamellar, L, and disordered network (solid line), N); 40% (network, N); 20% ($\sqrt{1}$:$\sqrt{3}$:$\sqrt{4}$:$\sqrt{7}$:$\sqrt{9}$:$\sqrt{12}$:$\sqrt{13}$:$\sqrt{16}$:$\sqrt{19}$:$\sqrt{21}$:$\sqrt{27}$:$\sqrt{28}$:$\sqrt{37}$:$\sqrt{48}$, hexagonal, $H_1$); 10% (disordered cylinders, C).

using a core–shell (bilayer) model with a core (PB) thickness $L$ = 15.4 and $\Delta L/L$ = 0.09 nm shown in Figure 7 (10 wt %). This calculation matches the experimental intensity at low $q$ values, including the first form-factor peak, but fails at higher scattering angles. This inconsistency at high $q$ values may reflect additional structure associated with the PEO corona but not accounted for in our simple model.

A third set of SAXS patterns has been taken from mixtures of water and OB9–1 ($w_{PEO}$ = 0.42), located at the center of the phase portrait (Figure 5). Figure 8 shows six scattering traces beginning with bulk OB9–1 (100 wt %), followed by dilution in regular increments down to a concentration of 10 wt %. The undiluted specimen contains the $H_2$ phase, which transforms to L between 70 and 90 wt % block copolymer; a representative SAXS pattern, obtained at 80 wt %, establishes this morphology. At 60 wt % the primary scattering peak broadens into what we interpret as the convolution of two reflections, hence a two-phase (L + N) region. Before evaluating the result at 40 wt %, we consider the 20 wt % SAXS data in Figure 8, which displays at least 12 orders of diffraction leading to the $H_1$ phase assignment found in Figure 5. At a composition of 10 wt %, OB9–1 is disordered, and the resulting SAXS pattern can be quantitatively modeled using a solid cylindrical form factor with $R_C$ = 16.2 nm and $\Delta R_C/R_C$ = 0.06 (solid curve, Figure 8).

The scattering pattern at 40 wt % in Figure 8 is unusual. It contains a primary peak at about $q^*$ = 0.01 Å$^{-1}$ but no clear higher order Bragg diffraction. At least two broad rounded peaks are evident at higher scattering wavevectors, which resemble form factor scattering. We obtained similar results from samples located throughout the region labeled N (identified by the dashed boundaries) in Figure 5. An earlier report[53] shows three additional such SAXS patterns taken from specimens located with the region labeled N in Figure 5 (samples OB9–1(26 wt %), OB9–11(35 wt %), and OB9–11(45 wt %), along with a fitted isotropic cylindrical form factor.

Between the L and $H_1$ phases in Figure 5 lies an extensive region of compositions and concentrations with structural features unlike either of the bordering states. Although the associated SAXS patterns lack long-range order, they more closely resemble the hexagonal phase than lamellae; note, in particular, the shape of the first-order peaks (in particular, see Figure 2 of ref 53). Significantly, the principal structural spacing changes only slightly between 20 and 45 wt % block copolymer. Moreover, the higher wavevector scattering is remarkably well accounted for using a hard cylinder form factor.[61,62] As shown below, we have determined that the morphology within the N region of the phase map corresponds to a randomly interconnected network of cylindrical struts. Other disordered, bicontinuous, network-like morphologies, for example, as documented in the final stage of spinodal decomposition,[63] have been shown to produce a well-defined principal scattering peak and a shoulder at 2$q^*$, similar to the results found in Figure 8 (40%) and in ref 53.

*3.3.2.2. Cryo-SEM.* Samples were further characterized using cryogenic scanning electron microscopy (cryo-SEM), a powerful microscopy technique capable of imaging nanometer scale topographical features in concentrated fluids and soft solids. Contrast is obtained with this technique by subliming water from the surface layer of a cryofractured specimen, leaving behind the frozen material originally dispersed in the aqueous medium. Here we present selected cryo-SEM images, obtained from several hydrated OB9 specimens that augment those presented earlier,[53] to establish the morphologies associated with mixtures within and around the N region identified in Figure 5. A more comprehensive treatment of the extensive set of cryo-SEM data obtained across the complete phase portrait will be separately published.

First, we assess microscopic evidence obtained from specimens with compositions outside the N region in Figure 5. Figure 9a shows a cryo-SEM image of a 25 wt % mixture of OB9–11 ($w_{PEO}$ = 0.39) in water. The predominant structural feature in this image is cylindrical, with little evidence of branches or spherical nodules. Although it is impossible to determine the aspect ratio with any certainty, these cylinders appear to be rather long, with length-to-radius exceeding at least 30−40. These cylinders are significantly more curved than those shown earlier[53] for the 20% OB9–1($w_{PEO}$ = 0.42) specimen.

At higher polymer concentrations, 60 wt % OB9–4 ($w_{PEO}$ = 0.34), a terraced morphology in the cryo-SEM image (Figure 9c) clearly reinforces the assignment of a lamellar morphology. This picture also agrees with our prior result (obtained with 50 wt % OB9–15 ($w_{PEO}$ = 0.30)).[53]

Between the hexagonal (cylindrical morphology) and lamellar phases lies the region labeled N (Figure 5). A cryo-SEM picture, obtained from a 30 wt % specimen of OB9–1 ($w_{PEO}$ = 0.42) is presented in Figure 9b. This image reveals a densely connected, random, network morphology. Strands of block copolymer, roughly 200−300 nm in length, are linked together at junctions that range from simple 3-fold unions to larger, flat, multifunctional connections. The basic structural element of the random network appears to be approximately cylindrical, with a diameter of 34–38 nm, consistent with the dimension extracted from the form factor scattering,[53] which was calculated based on a cylinder diameter of 32 nm. (Note that the structures evident in the cryo-SEM pictures contain both the PB (core) and PEO (shell) blocks, whereas the SAXS patterns reflect primarily core scattering).

The stability of the N morphology was tested by analysis of samples after extended annealing (room temperature for two weeks) and thermal cycling (five cycles per day between room temperature and 60 °C for two days). No perceptible changes were documented in the SAXS or cryo-SEM measurements after annealing the samples. Also, no changes were recorded when selected solutions were examined six months after preparation.

*3.3.2.3. Dynamic Mechanical Spectroscopy.* Figure 10 compares the linear visco-elastic properties of OB9–4 ($w_{PEO}$ = 0.34) mixtures at concentrations between 1 wt % and 40 wt % and a

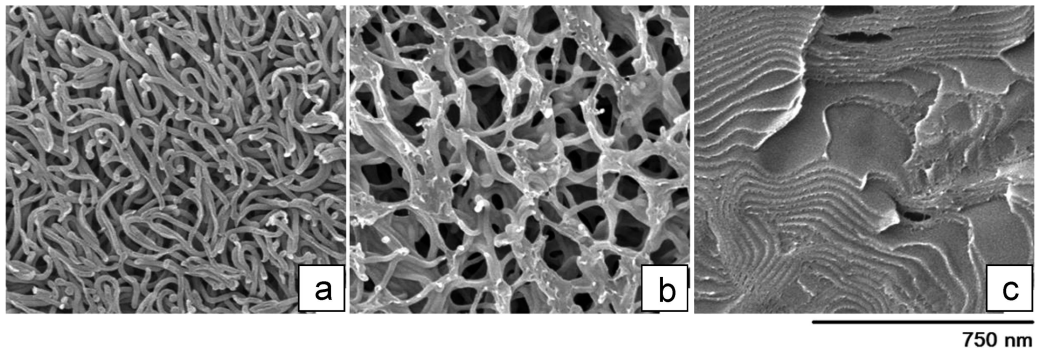


**Figure 9.** Representative cryo-SEM micrographs obtained from: (a) 25% OB9–11 ($w_{PEO} = 0.39$) exhibiting linear cylindrical structure; (b) 30% OB9–1 ($w_{PEO} = 0.42$) exhibiting a dense, network structure; and (c) 60% OB9–4 ($w_{PEO} = 0.34$) exhibiting a lamellar morphology.

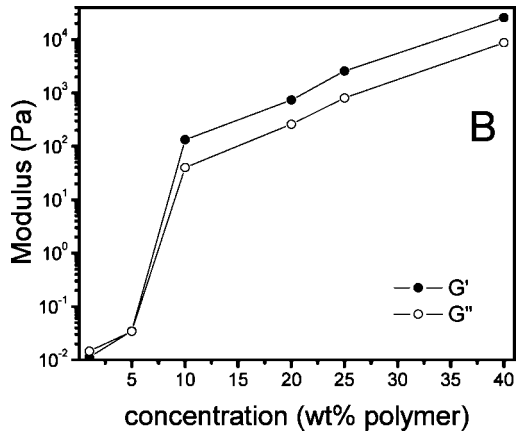


**Figure 10.** G′ and G″ as a function of the concentration of OB9–4 in water at 25 °C. The steep increase in modulii corresponds to the development of a contiguous network morphology.

frequency of 1 rad/sec; G′ and G″ is nearly independent of frequency between 0.1 and 100 rad/sec. The elastic and loss moduli increase dramatically upon increasing the copolymer concentration, with G′ and G″ rising more than 3 orders of magnitude between 5 wt % and 10 wt %. This copolymer self-assembles into the branched network structure (N) that coexists with water at low concentrations. The dramatic increase in moduli suggests transformation to a soft, gel-like solid consistent with the formation of a network morphology that spans the specimen.

*3.3.3. Packing Characteristics.* Structural details for the various morphologies such as the domain spacing ($d = 2\pi/q^*$), interfacial area per chain ($a_o$), and the characteristic size of the hydrophobic domain (sphere radius $R_S$, cylinder radius $R_C$, and core bilayer thickness $l_B$) can be estimated from SAXS measurements. These parameters were calculated using expressions provided elsewhere.[64] The interfacial area per chain and characteristic length for the network morphology were estimated assuming a hexagonal phase because the network represents an irregular state to which conventional packing laws could not be applied. Also, the hexagonal phase represents the closest analog to the N morphology as they both have a cylindrical structural motif. As water is added to the copolymer, the primary peak position ($q^*$) shifts toward lower $q$ values (Figures 2−4 and 6−8), indicating an increase in the domain spacing. Figure 11 summarizes the swelling behavior for a subset of the low and high molecular weight series copolymers as a function of the extent of hydration; the complete set of results may be found elsewhere.[65] For the OB1 series, the $d$-spacing ranges between 94 and 147Å in the melt state and between 279 and 343 Å for the 20% copolymer samples. Similar measurements for the OB9 series yielded lattice spacings ranging from 262 to 389 Å in

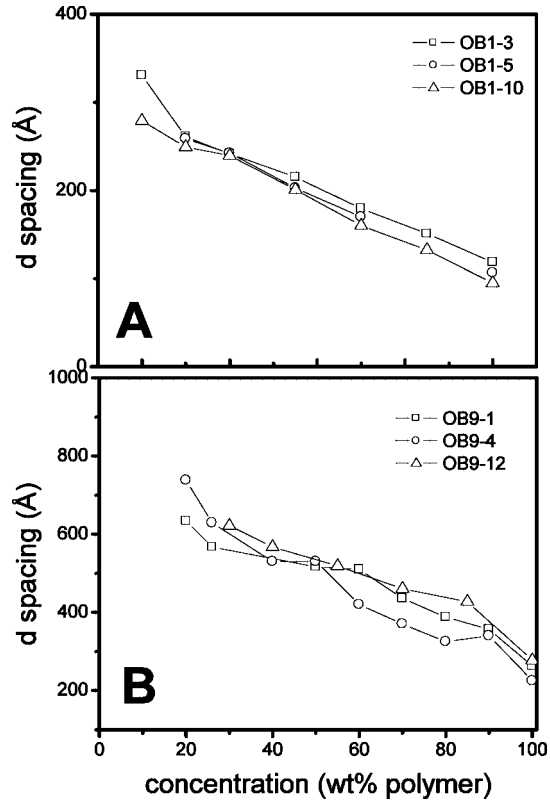


**Figure 11.** Domain size extracted from SAXS measurements for representative (A) OB1 and (B) OB9 mixtures with water. This parameter is relatively insensitive to variations in morphology and block copolymer composition ($w_{PEO}$).

the melt state and from 633 to 794 Å for the 20% copolymer samples. All of the copolymers swell to lattice dimensions (as expressed through $q^*$) that exceed twice the original size. Surprisingly, there are no signs of morphological changes in these data. (Figures 11A and 11B).

Calculated interfacial areas per chain for the OB1 and OB9 series are illustrated in Figures 12A and 12B, respectively. Unlike the $d$-spacing, the interfacial area per chain changes discontinuously when the morphology changes. However, the interfacial area per chain increases monotonically with hydration for a given ordered morphology. The interfacial area per chain for OB1–5 and OB9–11 decreases discontinuously at the $H_2$ to L transition and undergoes a step increase when L transforms to $H_1$. For the OB1 series, the interfacial area per chain ranges between 60 and 100 Å$^2$ for the lamellar morphology and between 110 and 170 Å$^2$ for the hexagonal phases. Similar estimates for the OB9 series yields interfacial areas per chain from 75 to 125 Å$^2$ for the lamellar phases and from 175 to 250

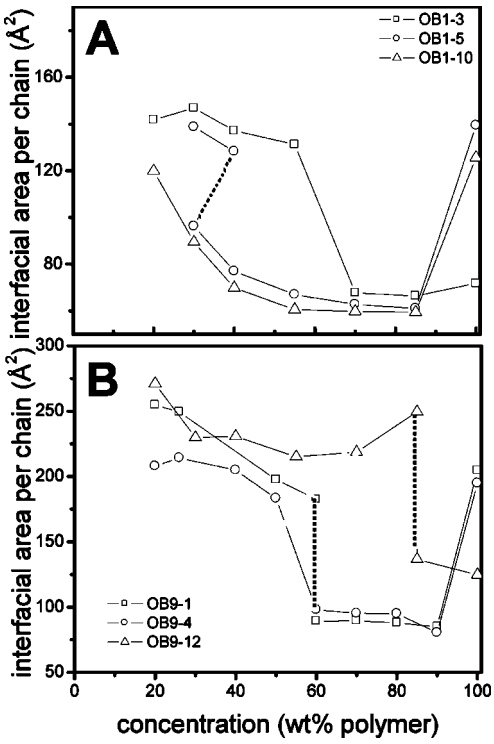


**Figure 12.** Interfacial area per chain determined for representative (A) OB1 and (B) OB9 samples as a function of the copolymer concentration. The dashed lines connect discontinuities associated with coexisting phases, resulting in two values of interfacial area per chain. Note, the interfacial area per chain for the network (N) samples was calculated assuming a cylindrical geometry.

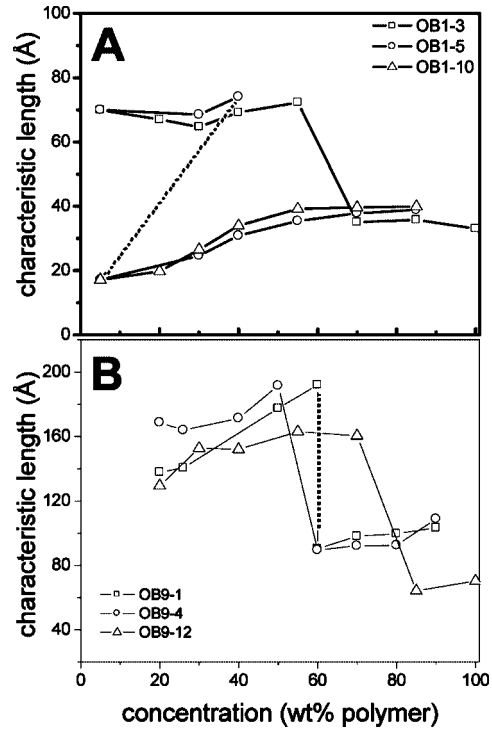


**Figure 13.** Characteristic length of the hydrophobic PB domains for (A) OB1 and (B) OB9 samples as a function of the copolymer concentration. The dashed lines identify discontinuities associated with coexisting phases. Note, the characteristic length for the N morphology was calculated assuming a cylindrical geometry.

Å$^2$ for the hexagonal phases (Figures 12A and 12B). The characteristic size of the hydrophobic (PB) domains ($R_S$, $R_C$, and $L_B$) decreases with decreasing copolymer concentration for a given morphology (Figures 13A and 13B). However, the characteristic dimension increases with the transition from lamellar (20 to 40 Å for OB1 series; 60 to 100 Å for OB9 series) to hexagonal (60 to 80 Å for OB1 series; 140 to 200 Å for OB9 series) as the water content increases.

## 4. Discussion

Two sets of amphiphilic block copolymers (OB1 and OB9) were examined at intermediate concentrations in water. Three types of isotropically dispersed morphologies—spheres (S), cylinders (C), and bilayer vesicles (B)—have been documented in both systems by cryo-TEM[45,46] for 1 wt % mixtures. These dispersed structures persist up to concentrations of about 10 wt % diblock copolymer, as shown by SAXS (Figures 1 and 5). In this limit, the SAXS patterns are dominated by form factor scattering, which has been satisfactorily modeled using mathematical expressions that account for the S (Figures 4 and 6), C (Figures 3 and 8), and B (Figures 2 and 7) geometries.[61,62] For the OB1 series, the dispersed morphologies resemble those reported for conventional surfactants and conform to well-established packing principles;[37,64] that is, the asymmetry of an amphiphilic molecule governs the interfacial curvature. Increasing molecular asymmetry (i.e., larger PEO blocks) is accommodated by morphological transitions from bilayers to cylinders to spheres.

The OB9 diblock copolymers exhibit additional, and significantly different, morphological features from the OB1 compounds at low concentrations. Increasing the core (PB) molecular weight leads to the emergence of a new structural unit, branches, or Y-junctions, at block copolymer compositions intermediate to those associated with bilayers and cylinders. In the limit of low concentrations (defined in Figure 5 by the dashed boundary running from about 25 wt % ($w_{PEO} = 0.24$) to 5 wt % ($w_{PEO} = 0.70$), branched cylindrical micelles are readily dispersed in water. However, within a narrow range of compositions, around $w_{PEO} = 0.34$, high levels of branching lead to the formation of a network morphology, resulting in macroscopic phase separation.[45] Tie lines in this region of the phase map, between 0 wt % and about 20 wt % (Figure 5), identify coexistence between the network (N) state and essentially pure water.

In contrast to spheres, cylinders, and vesicles, there is no way to continuously expand (dilate) a three-dimensional network formed from bulk (hydrophobic) cylindrical struts and multifunctional branches. Dispersion of the OB9–4 block copolymer requires vigorous mixing (e.g., sonication), which leads to the formation of network fragments.[45] These "network micelles" are stabilized by an extremely low critical micelle concentration (CMC), which inhibits exchange of diblock copolymer. Cryo-TEM analysis of these (nonequilibrium) network dispersions has provided the opportunity to characterize the local structure of the new network (N) phase in detail. Only three structural units were identified in this manner: Y-junctions, closed cylindrical loops, and spherical end caps. On the basis of these observations, we have deduced that the preferred local structure is dominated by Y-junctions, thus leading to the formation of a dense network under equilibrium conditions. This conclusion is supported by the macroscopic phase separation of the N state from essentially pure water, that is, when the fragmented network micelle dispersion was permitted to respond to the action of gravity. Over the period of several days, the network micelles rise to the top of the container and slowly fuse into a highly reticulated three-dimension labyrinth. On the basis of the location of the N region identified in Figure 5, we believe the equilibrium block copolymer concentration in the resulting N phase (see below) in macroscopically phase separated solutions of OB9–4 is approximately 25 wt %.

The extent of cylinder branching appears to be controlled by both $w_{PEO}$ and the block copolymer molecular weight. As discussed in a previous report,[45] we believe branching in cylindrical micelles is suppressed at low molecular weights due to the chain packing constraints associated with the formation of Y-junctions. However, we are unaware of any theoretical basis for associating this effect with either the packing of core (PB) blocks or the state of corona (PEO) hydration, or both. In an earlier publication[66] we showed that PEO blocks in OB dispersions partly collapse around micelle (spheres and cylinders) cores, presumably to shield unfavorable interactions at the hydrocarbon–water interface. This may contribute to the formation of cylindrical branches at higher molecular weights. Understanding branching in these amphiphilic systems will require additional, detailed, theoretical insights.

At a certain block copolymer composition (around $w_{PEO} = 0.34$), branches become the predominate structural element. Extended morphologies can be created by connecting 3-fold branches, either periodically or randomly. Two familiar examples of periodic structures are hexagonally perforated layers (HPL) (or graphite) and the gyroid, characterized by 3-fold connector angles of 0 and 70.5°, respectively. Cryo-TEM images of network fragments seem to favor a graphite-like structural motif,[45] although we cannot rule out the possibility that the confining environment associated with the experiment (i.e., a 0.2−0.3 $\mu$m thick film) biases the distribution of fragment topologies accessed with this technique. Nevertheless, we find numerous examples of planar and nonplanar placement of Y-junctions, leading us to conclude that the energetic difference between these arrangements must be quite subtle. Here again, theory is needed.

The most striking effects revealed by comparing the phase behavior of the OB1 (Figure 1) and OB9 (Figure 5) systems are found at intermediate concentrations. These illustrations reveal a new "phase", the disordered network (N), which occurs over a large range of compositions and concentrations in the higher molecular weight system (OB9). On the basis of close agreement between the SAXS patterns at higher $q$ values, obtained from specimens in the network region, and the calculated cylindrical form factor, along with the overall features evident in the cryo-SEM images, we conclude that the N phase represents an extended version of the network micelles described above. A soft-solid-like dynamic mechanical behavior (Figure 10) reinforces this conclusion.

Apparently, the molecular packing constraints imposed at intermediate concentrations ($0.20 \leq$ wt % polymer $\leq 0.50$) broadens the range of diblock compositions ($0.30 \leq w_{PEO} \leq 0.50$) that support extensive branching, resulting in the observed network formation. To the best of our knowledge, the N phase has not been anticipated by polymer-based theory (see below), and we are not able to intelligently speculate on the molecular factors that may be responsible for stabilizing this fascinating structure. Its absence at $N_{PB} = 46$ and appearance at $N_{PB} = 170$ parallels the development of cylindrical branching at low concentrations; therefore, we conclude that this new structural feature underpins network formation over the extensive range of the parameter space shown in Figure 5.

However, careful examination of numerous cryo-SEM images such as the one shown in Figure 9b suggests qualitative differences between the network structure in OB9–1 ($w_{PEO} = 0.42$) at concentrations of 26 and 30 wt % and the arrangement of Y-junctions documented by cryo-TEM for the OB9–4 ($w_{PEO} = 0.34$) network fragments. The former appears to be a looser structure, which may be correlated with less branching in the dilute limit. Other significant morphological differences have been discovered in and around the N region through extensive cryo-SEM experimentation and will be presented in a separate publication.[67]

On the basis of our analysis of the experimental results documented in this report, we tentatively conclude that the region in Figure 5 identified as N reflects a thermodynamically driven tendency to form a highly branched network morphology. However, we cannot state with any degree of certainty whether this represents an equilibrium or metastable state. Although a propensity to form highly branched cylindrical structures has been firmly established at low concentrations, the effects of nonergodicity, and topological barriers to structural reorganization, cannot be overlooked when considering the stability of the N phase. Nevertheless, such speculated impediments have not kept specimens bordering the N phase at intermediate concentrations, and with $H_1$ and L symmetry, from achieving long-range order. Moreover, selected specimens have been shown to be stable for extended periods of time (9 months), indicative of metastability or equilibrium. We will further explore this aspect of the network state in future work.

Most of the structural features reported here are anticipated by theoretical predictions for ternary surfactant mixtures by Tlusty et al.[54] Certain phenomenological details, including the sequence of topological transitions, S−C−$C_Y$−N−B, and the phase separation of branched structures in the dilute regime, are remarkably consistent with our experimental findings. Structural details such as the local geometry of 3-fold cylindrical Y-junctions suggest fundamental similarities between both amphiphilic systems. However, there also exist qualitative differences. We have described the phase behavior of two-component systems of diblock copolymer and water. Tlusty et al. deal with three-component, surfactant/water/oil, microemulsion mixtures that contain comparable amounts of surfactant and oil.

Structurally, Y-junctions can be represented by a lamellar bilayer bounded by three toroidal cylinders.[68] This hybrid structure necessitates different chain packing lengths and interfacial curvatures, possibly leading to a state of frustrated packing. We postulate that the conformational freedom associated with high molecular weight PB blocks enables the chains to act as a self-solvent, easing the constraints on domain packing in complex geometries such as the Y-junctions. Y-branching in the low molecular weight surfactant system is facilitated by the addition of oligomeric oil, which is not confined to the microdomain interface. This hypothesis regarding frustrated chain packing is supported by our previous identification of more complex interdomain geometries, including bilayer−cylinder junctions, in binary mixtures of polymeric surfactants.[46]

Superficially, the random network morphology appears to resemble the lamellar sponge morphology ($L_3$), documented in ternary surfactant systems,[69] and related structures in aqueous solutions of amphiphilic block copolymers.[49,51] However, the sponge morphology is a liquid-like disordered phase formed from sheet-like bilayer elements with close to zero-mean curvature and negative Gauss curvature.[40] Unlike the $L_3$ phase, the basic structural building block for the N morphology is cylindrical, which also results in nonzero mean curvature, along with negative Gaussian curvature. However, the N phase is located between the $H_1$ and L phases, whereas the $L_3$ sponge phase usually occupies a narrow slice of compositions between ordered lamellae and pure water. On the basis of these observations we conclude that the N phase reflects a fundamentally different state of self-assembly than $L_3$.

The network morphology appears to be related to the gyroid (Ia3d) structure, which also has been documented to occur between the H and L phases.[58] However, unlike the gyroid, the N phase is a disordered morphology. We believe this lack of

order may be driven by the entropically favorable irregular placement of the branch points.

Finally, two limiting examples of the packing of spheres should be noted: BCC in undiluted OB9–6 (Figure 5) and FCC for OB1–4 at 20 and 30 wt % (Figure 1). This difference reflects the consequences of soft and hard repulsive potentials, respectively, investigated by many research groups.[14,20,21,70,71] Long corona blocks tend to soften the interaction potential, whereas spheres with shorter corona blocks behave more as hard spheres and tend to pack onto a FCC lattice. Thermodynamic arguments suggest that, at intermediate concentrations, the PEO chains should be stretched normal to the interface and provide relatively soft interactions,[21] in contradiction to what we report for OB1–4. This interesting finding may be another manifestation of PEO chain collapse at the interface,[66] which would tend to harden the interaction potential.

## 5. Summary

SAXS, cryo-SEM, cryo-TEM, and dynamic mechanical spectroscopy were employed to study the phase behavior of PEO-PB (OB) diblock copolymers mixed with water, as a function of concentration (wt % copolymer in water) and block copolymer composition (fraction PEO). Self-assembly behavior was explored over three composition regimes: undiluted melts, intermediate concentrations, and as dilute dispersions. Two complete phase portraits were established, corresponding to degrees of PB polymerization $N_{PB} = 46$ and 170, and weight fractions of PEO ranging from 24 to 70%. At $N_{PB} = 45$, three structural motifs—spheres, cylinders, and bilayers—dominate the ordered and disordered regions of the phase portrait. Increasing $N_{PB}$ to170 results in the formation of a new type of network morphology, comprised of a random arrangement of interconnected (branched) cylinders, in addition to the other classical structures. This network phase, which occurs over a sizable range of compositions ($0.28 \leq w_{PEO} \leq 0.5$) and concentrations (26−50 wt % diblock copolymer), is characterized by a lack of translational order (as evidenced by SAXS and cryo-SEM) and a solid-like dynamic elastic modulus.

These findings reinforce the notion that increasing the molecular weight of nonionic surfactants leads to qualitative changes in the thermodynamics of self-assembly in aqueous solution. Specifically, cylinder branching is favored at higher molecular weights at compositions intermediate to those associated with bilayer (vesicles and lamellae) and straight cylinder formation. We believe that branching interferes with the development of long-range order, resulting in the formation of a random network morphology.

**Acknowledgment.** This work was supported primarily by the MRSEC Program of the National Science Foundation under Award No. DMR-0212302.

## References and Notes

(1) Israelachvili, J. In *Physics of amphiphiles: Micelles, Vesicle and Microemulsions*; Italian Physical Society: New York, 1983.
(2) Discher, B. M.; Burmudez, H.; Hammer, D. A.; Discher, D. E.; Won, Y.-Y.; Bates, F. S. *J. Phys. Chem. B* **2002**, *106*, 2848.
(3) Won, Y.-Y.; Paso, K.; Davis, H. T.; Bates, F. S. *J. Phys. Chem. B.* **2001**, *105*, 8302.
(4) Bermudez, H.; Brannon, A. K.; Hammer, D. A.; Bates, F. S.; Discher, D. E. *Macromolecules* **2002**, *35*, 8203.
(5) Leibler, L. *Macromolecules* **1980**, *13*, 1602–1617.
(6) Foerster, S.; Berton, B.; Hentze, H. P.; Kraemer, E.; Antonietti, M.; Lindner, P. *Macromolecules* **2001**, *34*, 4610–4623.
(7) Wright, E. R.; Conticello, V. P.; Apkarian, R. P. *Microsc. Microanal.* **2003**, *9*, 171–182.
(8) Bendejacq, D.; Ponsinet, V.; Joanicot, M.; Loo, Y. L.; Register, R. A. *Macromolecules* **2002**, *35*, 6645–6649.
(9) Goltner, C. G.; Henke, S.; Weissenberger, M. C.; Antonietti, M. *Angew. Chem., Int. Ed.* **1998**, *37*, 613–616.
(10) Braun, P. V.; Osenar, P.; Stupp, S. I. *Nature (London)* **1996**, *380*, 325–328.
(11) Puvvada, S.; Baral, S.; Chow, G. M.; Qadri, S. B.; Ratna, B. R. *J. Am. Chem. Soc.* **1994**, *116*, 2135–2136.
(12) Desai, S. D.; Gordon, R. D.; Gronda, A. M.; Cussler, E. L. *Curr. Opin. Colloid Interface Sci.* **1996**, *1*, 519–522.
(13) Balsara, N. P.; Stepanek, P.; Lodge, T. P.; Tirrell, M. *Macromolecules* **1991**, *24*, 6227–6230.
(14) McConnell, G. A.; Gast, A. P. *Macromolecules* **1997**, *30*, 435–444.
(15) Wanka, G.; Hoffmann, H.; Ulbricht, W. *Colloid Polym. Sci.* **1990**, *268*, 101–117.
(16) Wanka, G.; Hoffmann, H.; Ulbricht, W. *Macromolecules* **1994**, *27*, 4145–4149.
(17) Svensson, B.; Olsson, U.; Alexandridis, P. *Langmuir* **2000**, *16*, 6839–6846.
(18) Alexandridis, P.; Zhou, D.; Khan, A. *Langmuir* **1996**, *12*, 2690–2700.
(19) Svensson, M.; Alexandridis, P.; Linse, P. *Macromolecules* **1999**, *32*, 637–645.
(20) McConnell, G. A.; Gast, A. P.; Huang, J. S.; Smith, S. D. *Phys. Rev. Lett.* **1993**, *71*, 2102–2105.
(21) Hamley, I. W.; Daniel, C.; Mingvanish, W.; Mai, S.-M.; Booth, C.; Messe, L.; Ryan, A. J. *Langmuir* **2000**, *16*, 2508–2514.
(22) Hillmyer, M. A.; Bates, F. S. *Macromolecules* **1996**, *29*, 6994–7002.
(23) Esswein, B.; Moeller, M. *Angew. Chem., Int. Ed. Engl.* **1996**, *35*, 623–625.
(24) Foerster, S.; Kraemer, E. *Macromolecules* **1999**, *32*, 2783–2785.
(25) Zhang, L.; Eisenberg, A. *Science* **1995**, *268*, 1728–1731.
(26) Zhang, L.; Eisenberg, A. *J. Am. Chem. Soc.* **1996**, *118*, 3168–3181.
(27) Hentze, H. P.; Kraemer, E.; Berton, B.; Foerster, S.; Antonietti, M.; Dreja, M. *Macromolecules* **1999**, *32*, 5803–5809.
(28) Messe, L.; Corvazier, L.; Young, R. N.; Ryan, A. J. *Langmuir* **2002**, *18*, 2564–2570.
(29) Deng, Y.; Young, R. N.; Ryan, A. J.; Fairclough, J. P. A.; Norman, A. I.; Tack, R. D. *Polymer* **2002**, *43*, 7155–7160.
(30) *Amphiphilic Block Copolymers: Self-Assembly and Applications*; Alexandridis, P., Lindman, B. Eds.; Elsevier: Amsterdam, 2000.
(31) Borchert, U.; Lipprandt, U.; Bilang, M.; Kimpfler, A.; Rank, A.; Peschka-Suss, R.; Schubert, R.; Lindner, P.; Förster, S. *Langmuir* **2006**, *22*, 5843.
(32) Stoenescu, R.; Meier, W. *Chem. Commun.* **2002**, 3016.
(33) Long, J. W.; Logan, M. S.; Rhodes, C. P.; Carpenter, E. E.; Stroud, R. M.; Rolison, D. R. *J. Am. Chem. Soc.* **2004**, *126*, 16879–16889.
(34) Castro-Roman, F.; Porte, G.; Ligoure, C. *Langmuir* **2001**, *17*, 5045–5058.
(35) Chen, S.-H.; Choi, S. *Supramol. Sci.* **1998**, *5*, 197–206.
(36) Seddon, J. M. *Biochim. Biophys. Acta* **1990**, *1031*, 1–69.
(37) Hyde, S. T.; Fogden, A. *Prog. Coll. Pol. Sci.* **1998**, *108*, 139–152.
(38) Appell, J.; Porte, G.; Khatory, A.; Kern, F.; Candau, S. J. *J. Phys. II* **1992**, *2*, 1045–1052.
(39) Sallen, L.; Sotta, P.; Oswald, P. *J. Phys. Chem. B* **1997**, *101*, 4875–4881.
(40) Strey, R.; Schomacker, R.; Roux, D.; Nallet, F.; Olsson, U. *J. Chem. Soc., Faraday Trans.* **1990**, *86*, 2253–2261.
(41) Ciach, A. *J. Chem. Phys.* **1996**, *104*, 2376–2384.
(42) Funari, S. S.; Rapp, G. *Proc. Natl. Acad. Sci.* **1999**, *96*, 7756–7759.
(43) Imai, M.; Kawaguchi, A.; Saeki, A.; Nakaya, K.; Kato, T.; Ito, K.; Amemiya, Y. *Phys. Rev. E.* **2000**, *62*, 6865–6874.
(44) Alexandridis, P.; Spontak, R. J. *Curr. Opin. Colloid Interface Sci.* **1999**, *4*, 130–139.
(45) Jain, S.; Bates, F. S. *Science* **2003**, *300*, 460–464.
(46) Jain, S.; Bates, F. S. *Macromolecules* **2004**, *37*, 1511–1523.
(47) Ryan, A. J.; Mai, S.-M.; Fairclough, J. P.; Hamley, I. W.; Booth, C. *Phys. Chem. Chem. Phys.* **2001**, *3*, 2961.
(48) Hamley, I. W.; Mai, S.-M.; Ryan, A. J.; Fairclough, J. P.; Booth, C. *Phys. Chem. Chem. Phys.* **2001**, *3*, 2972.
(49) Battaglia, G.; Ryan, A. J. *Nat. Mater.* **2005**, *4*, 869.
(50) Battaglia, G.; Ryan, A. J. *Angew. Chem., Int. Ed.* **2006**, *45*, 2052.
(51) Battaglia, G.; Ryan, A. J. *Macromolecules* **2006**, *39*, 798.
(52) Battaglia, G.; Ryan, A. J. *J. Phys. Chem. B* **2006**, *110*, 10272.
(53) Jain, S.; Gong, X.; Scriven, L. E.; Bates, F. S. *Phys. Rev. Lett.* **2006**, *96*, 138304.
(54) Tlusty, T.; Safran, S. A.; Strey, R. *Phys. Rev. Lett.* **2000**, *84*, 1244–1247.
(55) Bellare, J. R. Cryo-Electron and Optical Microscopy of Surfactant Microstructures. Ph.D. Thesis, University of Minnesota, Minneapolis, 1988.
(56) Talmon, Y. *Ber. Bunsen-Ges.* **1996**, *100*, 364–372.
(57) Rosedale, J. H.; Bates, F. S. *Macromolecules* **1990**, *23*, 2329–2338.
(58) Khandpur, A. K.; Förster, S.; Bates, F. S.; Hamley, I. W.; Ryan, A. J.; Bras, W.; Almdal, K.; Mortensen, K. *Macromolecules* **1995**, *28*, 8796.
(59) Won, Y.-Y.; Brannan, A. K.; Davis, H. T.; Bates, F. S. *J. Phys. Chem. B* **2002**, *106*, 3354–3364.
(60) Shen, H.; Eisenberg, A. *Macromolecules* **2000**, *33*, 2561–2572.

(61) Bang, J.; Jain, S.; Li, Z.; Lodge, T. P.; Pedersen, J. S.; Kesselman, E.; Talmon, Y. *Macromolecules* **2006**, *39*, 1199.
(62) Pedersen, J. S. *J. Appl. Crystallogr.* **2000**, *33*, 637–640.
(63) Jones, R. A.; Norton, L. J.; Kraemer, E.; Bates, F. S.; Wiltzius, P. *Phys. Rev. Lett.* **1991**, *66*, 1326–1329.
(64) Hajduk, D. A.; Kossuth, M. B.; Hillmyer, M. A.; Bates, F. S. *J. Phys. Chem. B* **1998**, *102*, 4269–4276.
(65) Jain, S. Aqueous Mixtures of Block Copolymer Surfactants. Ph.D. Thesis, University of Minnesota, 2005.
(66) Won, Y.-Y.; Davis, H. T.; Bates, F. S.; Agamalian, M.; Wignall, G. D. *J. Phys. Chem. B* **2000**, *104*, 9054.
(67) Gong., X.; Sumeet, J.; Scriven, L. E.; Bates, F. S. to be submitted.
(68) May, S.; Bohbot, Y.; Ben-Shaul, A. *J. Phys. Chem. B* **1997**, *101*, 8648–8657.
(69) Roux, D.; Coulon, C.; Cates, M. E. *J. Phys. Chem.* **1992**, *96*, 4174–4187.
(70) Lodge, T. P.; Bang, J.; Park, M. J.; Char, K. *Phys. Rev. Lett.* **2004**, *92*, 145501.
(71) Bang, J.; Lodge, T. P. *J. Phys. Chem. B* **2003**, *107*, 12071.

MA702322B